Hindawi
International Journal of RF and Microwave Computer-Aided Engineering
Volume 2023, Article ID 4859324, 10 pages
https://doi.org/10.1155/2023/4859324

Research Article

Design and Implementation of a Novel Radar Cross Section Reduction Metasurface Covering 12.5-17.4 GHz and 20.5-36.2 GHz

Mei-Lin Yu,[1] **Xi Hou**,[2] **and Yong-Hong Zhou**[2]

[1]*Sichuan Earthquake Administration, Chengdu 610000, China*
[2]*School of Electronic Info. Eng, China West Normal Univ., Nanchong 637000, China*

Correspondence should be addressed to Yong-Hong Zhou; scnczyh@163.com

Received 29 December 2022; Revised 30 June 2023; Accepted 28 July 2023; Published 1 September 2023

Academic Editor: Alessandro Di Carlofelice

Based on the theory of polarization conversion, this paper designs and implements two electromagnetic units with a 180-degree reflection phase difference in the range of 10-40 GHz. By coding and optimizing the spatial arrangement of the two basic units to obtain a metasurface, which makes the incident electromagnetic waves reflect diffusely, the energy in a single beam direction is reduced to realize the reduction of the radar cross section (RCS). The full wave simulated and experimental results of the reduction of the RCS of the metasurface have been presented. The RCS of the proposed metasurface can be reduced by more than 10 dB in the two broadband bands of 12.5-17.4 GHz and 20.5-36.2 GHz, and the maximum reduction can reach 26 dB, compared with a metallic surface of the same size. In addition, the optimized metasurface can also maintain a good reduction effect under oblique incident wave directions of 30, 45, 60, and 70 degrees. A very good agreement between simulation and measurement results is observed.

1. Introduction

Metasurfaces [1] are periodic or nonperiodic arrangements of unitary structures of specific geometries on the macroscopic subwavelength scale that break through the microscopic layout of atoms and molecules of natural materials and have unique electromagnetic properties. Examples include negative refractive index [2], near-zero magnetic permeability [3], and near-zero dielectric constant [4, 5]. And metasurfaces have also been extensively investigated for a variety of novel electromagnetic functions, such as polarization transformation [6, 7], holographic imaging [8, 9], perfect reflection [10, 11], and radar scattering cross section (RCS) reduction [12]. Along with the rapid development of aerospace, maritime technology, reconnaissance, and counter-surveillance technologies, the need for stealth materials [3, 13–16] is becoming more and more urgent. Compared to traditional techniques of changing the shape of the object or using absorbent coatings to reduce the RCS, supersurfaces [17–19] have the advantages of simple design, low cost, ground profile, and low loss, so metasurfaces have good prospects for development.

In recent years, researchers have proposed various types of metasurfaces that can achieve RCS reduction. Liu et al. proposed the use of a nonresonant metamaterial progenitor based on transformed optics [20], implemented by applying a conformal coordinate transformation to a system of Maxwell's equations to obtain an intrinsic dataset of the spatial distribution of the hypersurface; Priyanka and Kaushik proposed a unique split-square ring absorber to reduce RCS [21]; Su et al. proposed a novel nonuniform hierarchical coding [22] of metamaterial [23] tiles; Yang et al. proposed RCS reduction by scattering mechanism using carbon fiber-linked composites [24]; and Xu et al. proposed on an efficient Pancharatnam-Berry meta-atomic method to form subarrays with focused reflective phase profiles that can ensure almost uniform diffuse scattering of arbitrarily polarized electromagnetic waves to achieve RCS reduction [25–27], and a stealth strategy that uses ultrathin parabolic metasurfaces to achieve dual polarization channel and

multifrequency channel diffuse reflection stealth, allowing for fundamental wave number splitting and wave number splitting supersurfaces of scattered waves [28, 29]; Li et al. and Chen et al. proposed an optimized optically transparent metasurface for polarization and angle-insensitive broadband single-station as well as dual-station RCS reduction [30, 31]; Ying-jie et al. proposed an anisotropic metallic elliptical ring that modulates the intrinsic resonant phase by changing the structure of the superatom and integrates resonant phase and geometric phase modulation to excite diffusion-like scattering by scattering the electromagnetic energy in multiple directions to suppress specular RCS [32]. However, some of the above work only considers single-station RCS reduction and not the more important two-station RCS reduction, and most of the metasurface RCS reduction has a narrower band and a relatively more complex structure.

In this paper, we present a method to reduce the RCS using polarization-transformed supersurfaces operating in the ultrawideband frequency range. Polarization conversion is the process of converting the polarized state of an electromagnetic wave to another polarized state. By designing the shape, size, and arrangement of the supersurface unit as well as the material properties, the phase and amplitude of the electromagnetic wave can be modulated. The researchers designed two mirror-like electromagnetic cells and used a genetic algorithm to optimize their arrangement in the array. The results show that the proposed method achieves an RCS reduction of more than 10 dB in the ultrawide frequency range of 12.5-17.4 GHz and 20.5-36.2 GHz. The designed superstructure surface has the advantage of being easy to machine and flexible to manipulate, making it promising for electromagnetic stealth applications.

2. Materials and Methods

2.1. Unit Design. We propose a unique metasurface unit, based on the metal split ring patch and the rectangular metal patch; the unit's schematic is shown as illustrated in Figure 1. The unit comprises three layers: a rounded metal patch with a simple double gap and a small rectangular metal patch printed on the top surface of a dielectric substrate, a dielectric spacer, and a ground plate, from top to bottom. The dielectric substrate is made of PTFE with a thickness of 2 mm and a dielectric constant of 2.2. Both the metal patch and ground have a thickness of 0.018 mm, from top to bottom. The geometric parameters are as follows: $a = 5$ mm, $b = 0.9$ mm, $h = 2$ mm, $l = 1$ mm, $r = 2.2$ mm, and $t = 0.018$ mm.

Figure 2(a) displays the copolarized and cross-polarized scattered characteristics of the unit under the vertical incidence of x-polarized waves. In the frequency range of 12.4-38.1 GHz, the proposed unit can achieve a copolarized reflection coefficient of less than -10 dB, which includes four resonant valleys at 14 GHz, 23.5 GHz, 34 GHz, and 36.5 GHz. At each resonant valley, the copolarized reflection coefficient reaches its minimum value, indicating that the incident x-polarized wave is entirely converted into a

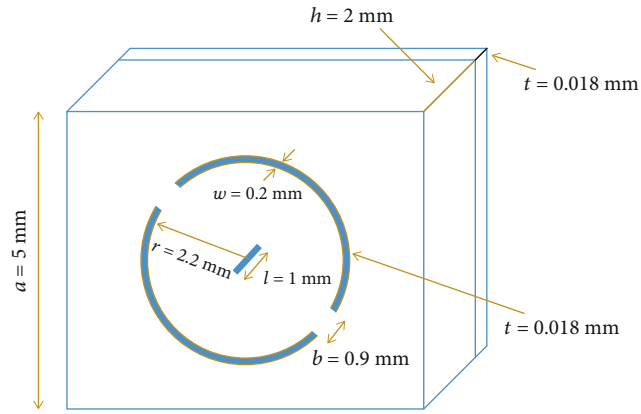

Figure 1: Schematic diagram of the structure of the polarization conversion unit.

y-polarized reflected wave. When an x-polarized electromagnetic wave is incident onto the unit, it is converted into a y-polarized electromagnetic wave, and the PCR [33] can be expressed as

$$\mathrm{PCR} = \frac{r_{yx}^2}{r_{yx}^2 + r_{xx}^2}. \tag{1}$$

Figure 2(b) illustrates the PCR of the unit in the frequency range of 12.4-38.1 GHz. It can be observed that the PCR is consistently above 90%. The PCR at the four resonant valleys is approximately 1, indicating an almost complete conversion of the unit's polarization direction.

When the polarization direction of the incident wave is converted by the polarization conversion unit, it results in a 90-degree phase shift. Additionally, in addition, the PB phase principle enables phase modulation by simply rotating the cell angle, and we mirror this supersurface cell to obtain another conversion cell that can bring about a phase shift of -90 degrees. Consequently, two units that are mirror images of each other will produce a phase difference of 180 degrees. The phase diagrams of the polarization conversion unit and its mirror unit, respectively, illustrate the phase difference of the reflection coefficient of the two units, which is approximately 180 degrees in a broad frequency band from 10 GHz to 40 GHz (see Figure 3). This meets the unit phase requirements of 1-bit encoding metamaterials. Therefore, we can simulate the two mirror-symmetric polarization conversion units as binary numbers "1" and "0" and apply them to the RCS reduction metasurface (see Figure 4).

2.2. Array Optimization Design for Reduced Surface. In 2014, Professor Tiejun Cui's team at Southeast University proposed the concept of an encoded metasurface based on electromagnetic metamaterials. This technology digitally encodes cells with a certain phase difference in reflection coefficients by defining the phase of cell reflection coefficients [33]. In this paper, we use a genetic algorithm, which is an adaptive probabilistic search algorithm for

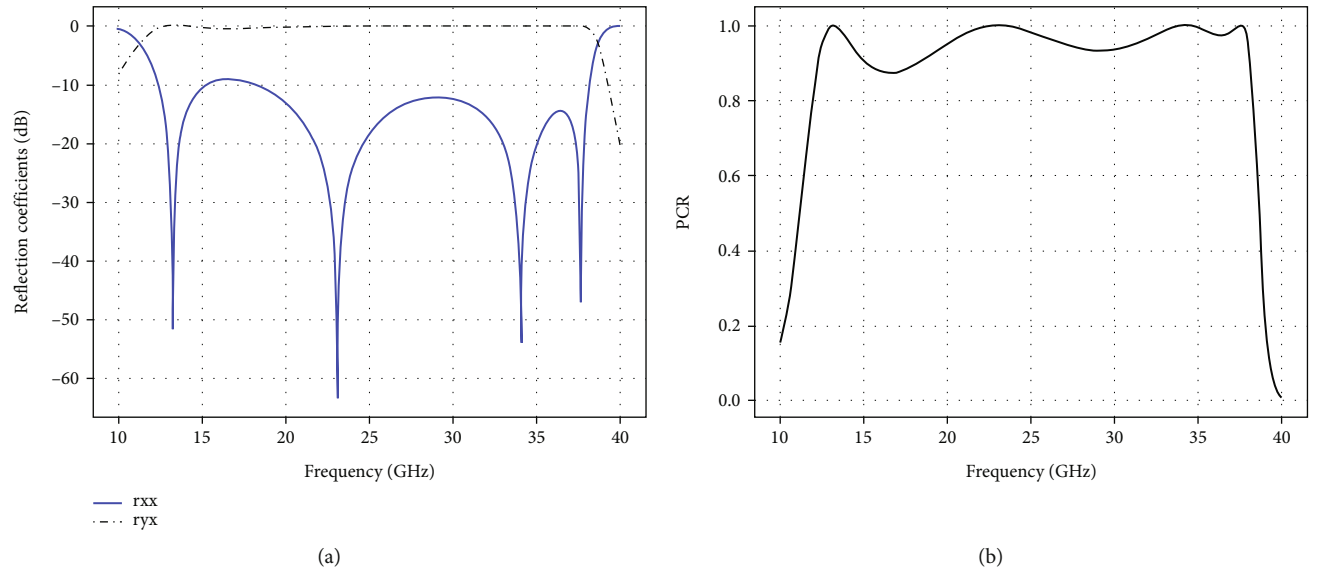

Figure 2: (a) Reflection coefficients for copolarization and cross-polarization. (b) PCR of polarization conversion unit.

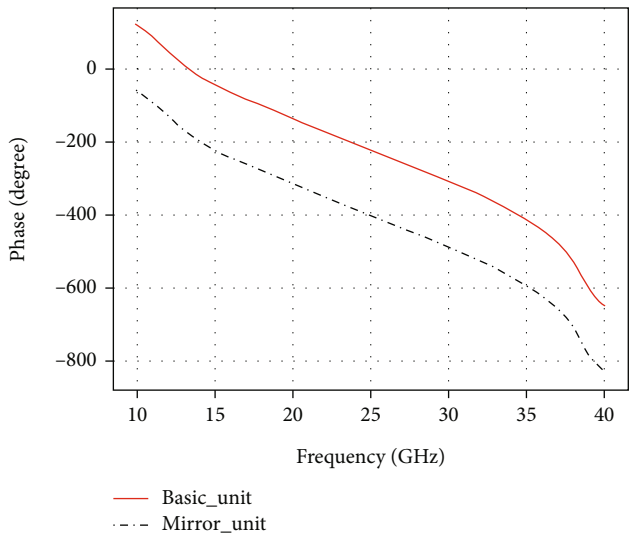

Figure 3: Phase curve diagram of the polarization reduction conversion unit and the mirror unit.

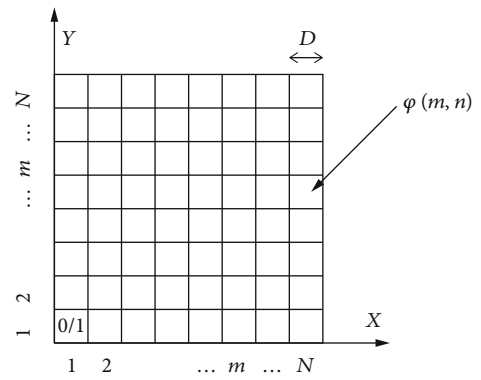

Figure 4: Schematic diagram of RCS reduction metasurface arrangement.

global optimization borrowed from the mechanism of natural selection and genetic laws of living organisms, to optimize the arrangement of encoded metasurfaces. Compared with the particle swarm optimization algorithm and artificial neural network optimization algorithm, the genetic algorithm has a strong global search capability, wider applicability, and supports multiobjective optimization [34, 35]. It is less likely to fall into local optimal solutions than the particle swarm algorithm and does not require a large amount of training data or computational resources like artificial neural network algorithms. Additionally, the computational rate is relatively fast, which makes it more suitable for optimizing the arrangement of supersurface array units proposed in this paper.

To obtain the units with stable phase, we used the 2*2 basic units as a supercell, and the supercell is considered as binary digital elements of "0" or "1"; see Figure 5. Based on the supercell, we designed an 8*8 metasurface. In the case of vertical incidence of electromagnetic waves, the far-field scattering of the metasurface can be expressed as

$$f(\theta,\varphi) = f_e(\theta,\varphi)\sum_{m=1}^{N}\sum_{n=1}^{N}\exp\left\{-i\left\{\varphi(m,n) + KD\sin\theta\left[\left(m-\frac{1}{2}\right)\cos\varphi + \left(n-\frac{1}{2}\right)\sin\varphi\right\}\right\}\right\}, \tag{2}$$

where φ and θ are the pitch and azimuth angles of the reflected wave, respectively, and is the directional function of the supercell. Here, m and n denote the number of rows and $f_e(\theta,\varphi)$ columns of the array, respectively, and $\varphi(m,n)$ denotes the scattering phase of the (m, n) supercell. $K = 2\pi/\lambda$ is the propagation constant, and D

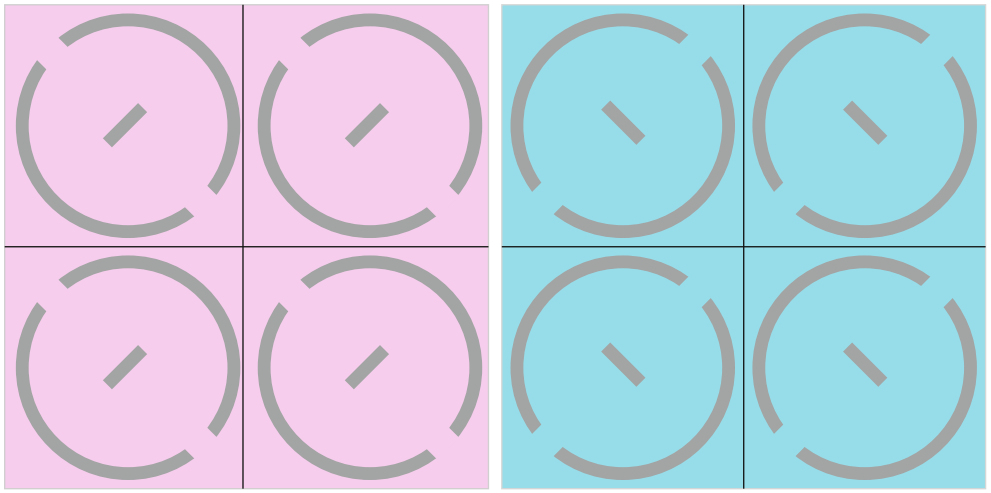

Figure 5: A depiction of the two-unit cells. The red part is element "0," and the blue part is element "1."

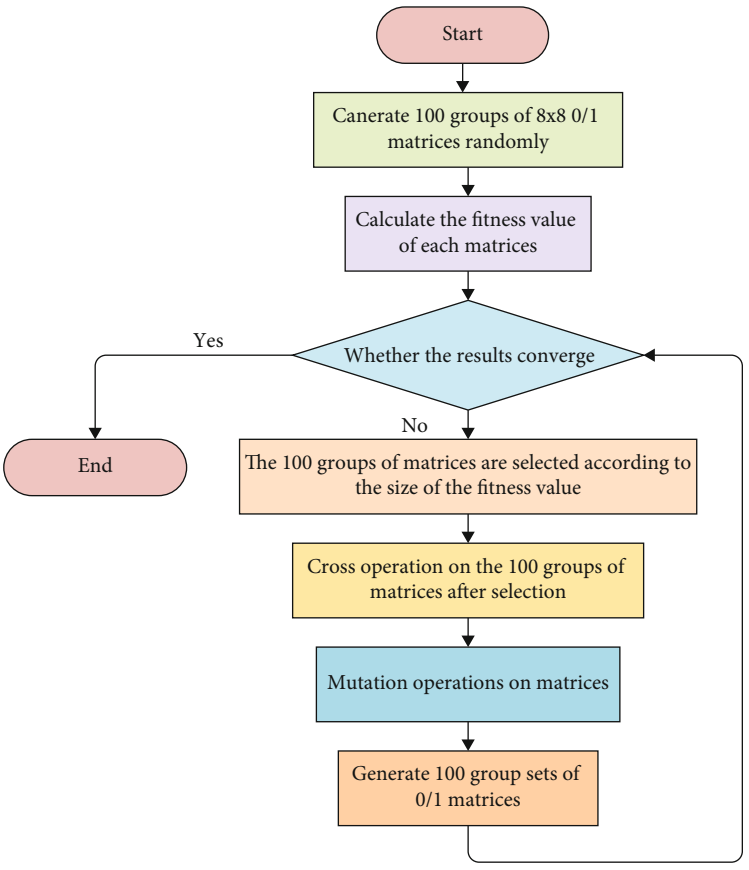

Figure 6: Optimized flow chart of genetic algorithm.

represents the length of a single supercell. We can calculate the far-field function value scattered by the metasurface with a given coding mode using Equation (2). The pointing function of a metasurface can be expressed [33] as

$$D_{ir}(\theta,\varphi) = \frac{4\pi|f(\theta,\varphi)|^2}{\int_0^{2\pi}\int_0^{\pi/2}|f(\theta,\varphi)|^2 \sin\theta d\theta d\varphi}. \quad (3)$$

Hence, to obtain the optimal RCS reduction for the 1-bit case, we use the genetic algorithm to optimize the coding array to find the metasurface with efficient RCS reduction. The fitness function is set as

$$f_{\text{fitness}} = \max\left(f(\theta,\varphi)\right). \quad (4)$$

Accordingly, the Python programming language is used to accomplish the optimization of the genetic algorithm for the

1	0	1	1	1	1	0	1
1	0	0	1	0	1	0	0
1	0	0	0	0	0	1	1
1	0	0	1	1	0	1	1
0	0	1	1	1	0	1	1
1	0	0	1	0	1	0	0
0	0	1	1	0	1	0	1
1	1	1	0	1	0	0	0

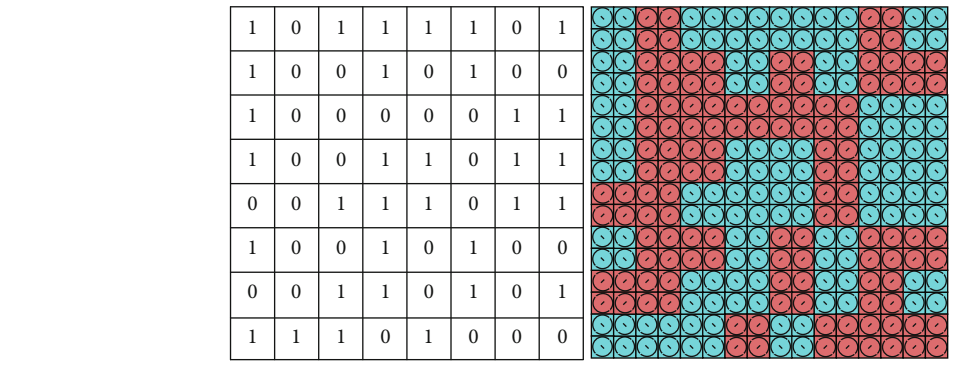

Figure 7: Optimized sequence of RCS reduction metasurface.

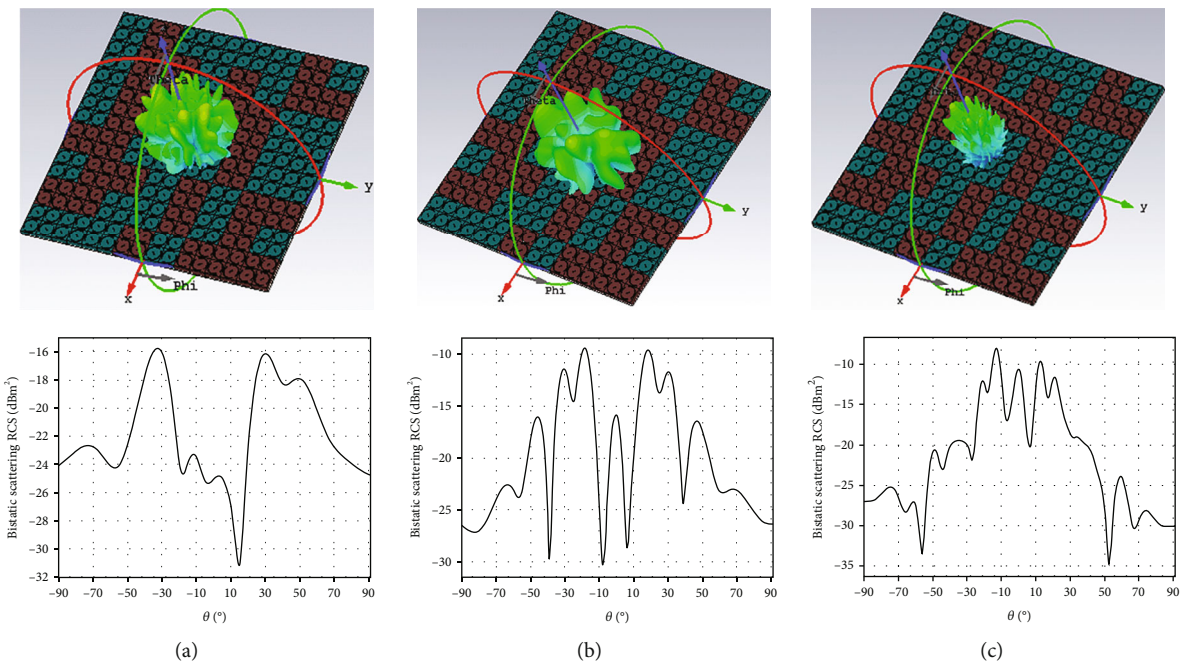

Figure 8: RCS under three different frequency points: (a–c) 14 GHz, 24 GHz, and 34 GHz.

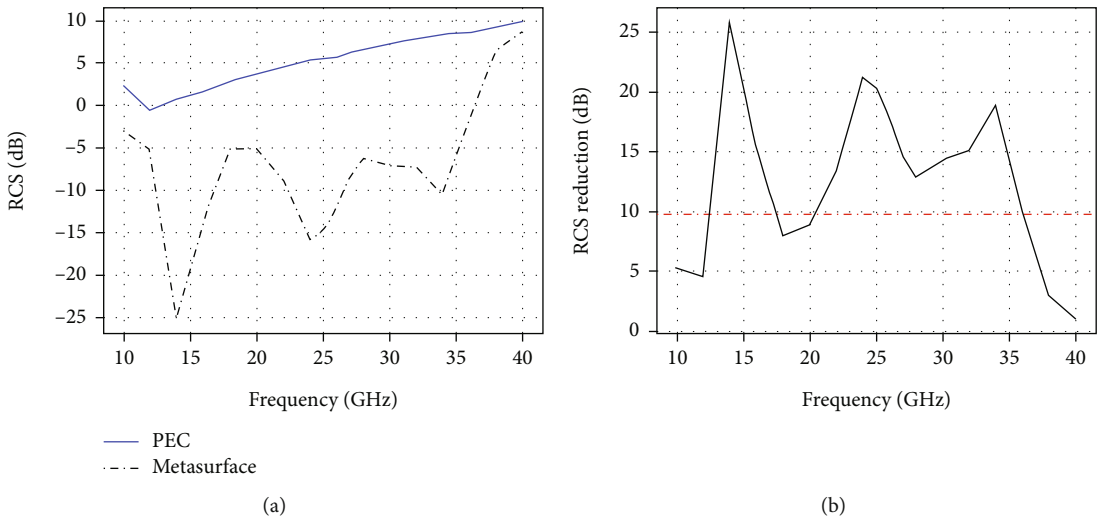

Figure 9: (a) Bistatic RCS of the metallic plate and reduction metasurface. (b) The simulation result of bistatic RCS reduction over a wide frequency range.

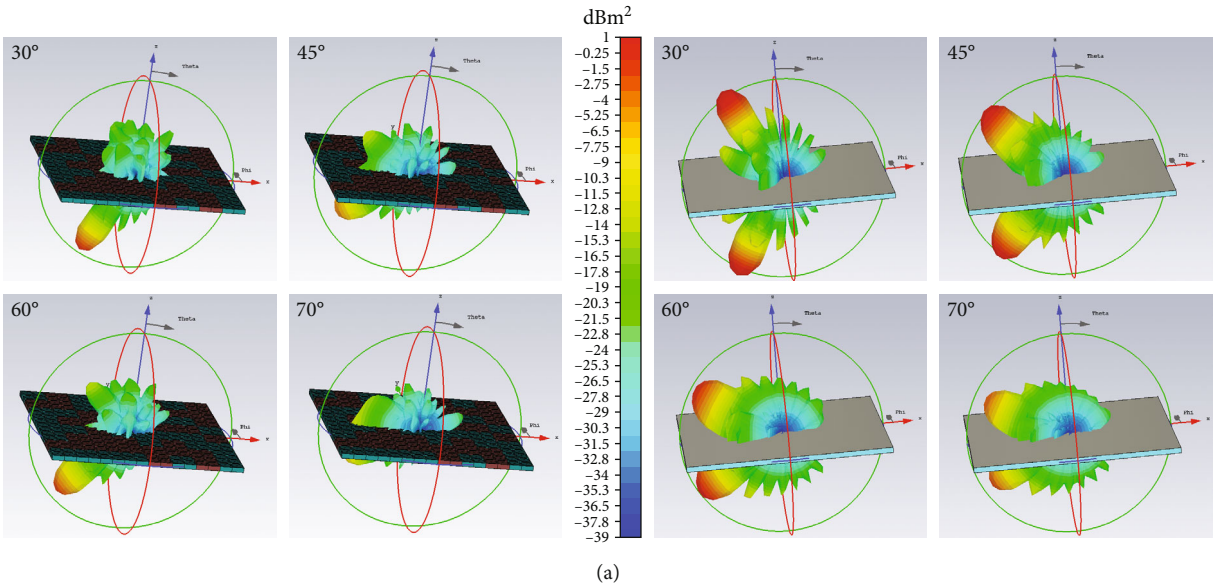

(a)

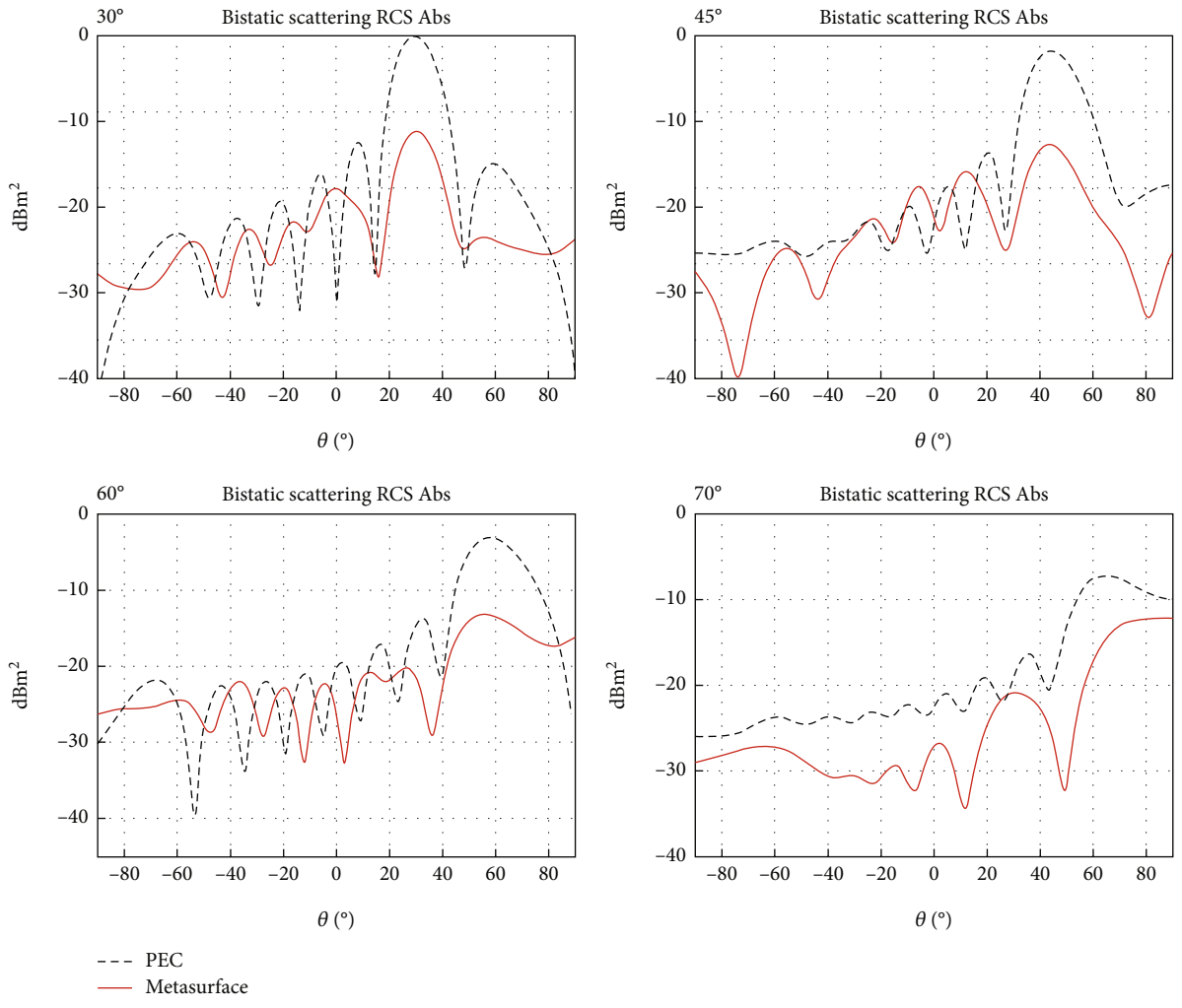

(b)

Figure 10: Comparative RCS plots for 4 different oblique incidence angles of the supersurface as well as the metal surface. (a) RCS far-field comparison chart. (b) RCS linearity comparison chart.

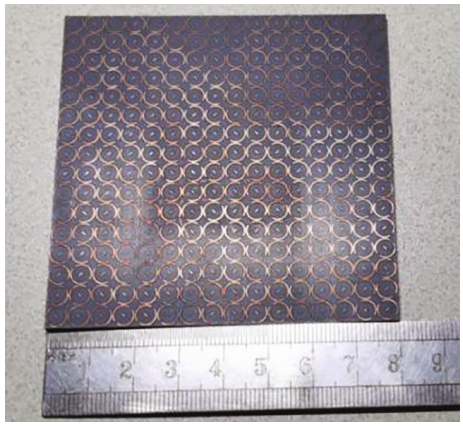

Figure 11: RCS reduced surface sample.

array of RCS reduction surfaces. Firstly, 100 groups of 8 × 8 0/1 matrices were randomly generated to represent the initial population. Each matrix is equivalent to a biological chromosome; then, fitness values were calculated for each set of randomly generated matrices. The matrices are selected for replication using a roulette wheel method, and matrices with higher fitness values have a greater probability of being selected. By mutating the selected matrix, the generated matrices can jump out of the local optimal solution. In this paper, the crossover probability is set to 0.9, and the mutation probability is set to 0.05. Finally, repeat the above steps for each group of newly generated matrices until the program runs through the set number of iterations to reach the convergence result. We provided the specific operation flow chart; see Figure 6.

The optimized arrangement of the 1-bit RCS reduction surface by the program is shown in Figure 7. The structure of the RCS reduction metasurface is modeled and numerously simulated by using the electromagnetic simulation software CST MICROWAVE STUDIO. The simulation results are shown in Figure 8.

The three-dimensional far-field diagram and Cartesian coordinate diagram of RCS at three frequency points, 14 GHz, 24 GHz, and 34 GHz, are selected for observation. Moreover, after the plane wave is incident vertically along the z-axis direction to the metasurface, the energy of the retroreflected lobe is no longer mainly concentrated in the normal direction of the z-axis but is diffusely reflected in numerous directions. The proposed RCS reduction metasurface effectively suppresses the appearance of strong reflection peaks.

To observe the reduction characteristics of the RCS reduction metasurface more clearly and intuitively, a metallic surface with the same structural size as the optimized metasurface is designed for comparison, and the electromagnetic parameters of the substrate of the metal plate are still the same as those of the metasurface. The RCS comparison results and RCS reduction values of both are shown in Figure 9.

As shown in Figure 8(a), the RCS values of the reduction metasurface are less than -10 dB in the two ranges of 12.5-17 GHz and 22.6-26.8 GHz. However, the RCS value of the metallic surface in the range of 10-40 GHz is almost more than 0 dB. In Figure 8(b), the optimized reduction metasurface reduces more RCS of 10 dB in the 12.5-17 GHz and 20.5-36 GHz frequency bands than the metallic surface of the same size. In the 17-20.5 GHz frequency band, the RCS reduction effect of the metasurface is relatively inferior, owning the low polarization conversion rate of the unit. At the frequency where the unit polarization conversion rate is close to 1, the metasurface plate reaches the local maximum of the RCS reduction.

In practical applications, the radar detection wave that the target object faces are not only a vertical incident wave but also the incidence of electromagnetic waves from different directions. Therefore, for the optimized RCS reduction metasurface, we set four different incident directions to test its RCS reduction effect, namely, 30 degrees, 45 degrees, 60 degrees, and 70 degrees. Figure 10 shows the scattering direction diagram of the reflected wave on the RCS reduction metasurface and the metal surface under four different angles of incidence at the frequency point of 15 GHz. We can observe that under different incident angles in Figure 9(a), the main lobe of the reflected wave of the RCS reduction metasurface also moves with the incident angle, and the effect of reducing the RCS is still significant, and the bistatic RCS remains below -10 dB. We can observe from the curve chart in Figure 9(b) that the RCS reduction effect of our designed metasurface is significant compared with metallic surfaces at incident angles of 30, 45, 60, and 70 degrees.

3. Experimental Testing and Analysis

To verify the effectiveness of the RCS reduction metasurface, we designed and fabricated an RCS reduction metasurface sample. The size of the sample is the same as the simulation model, and the sample is shown in Figure 11. The size of the entire metasurface is 80 mm × 80 mm, and the material used for the dielectric substrate is PTFE with a thickness of 2 mm and a dielectric constant of 2.2. Moreover, both the ground plate and the top layer patch are made of metal copper with a thickness of 0.018 mm. Placing the sample in the center of the test bench and fixing the horn antenna in the vertical direction is the plane wave feed. The port of the vector network analyzer is connected to the horn antenna through the feeder to measure the RCS of the sample.

The experimental test environment and equipment are shown in Figure 12(a), Figure 12(b) is the test environment of the sample plate in the microwave darkroom using the horn antenna to transmit the signal in the low-frequency band of 8-18 GHz, and Figure 12(c) is the test environment of the sample plate in the high-frequency band of 18-40 GHz in the dark room. Figure 13(a) is the RCS reduction data of the sample plate and the metal plate measured experimentally. It indicates that the data at 18 GHz are incoherent due to the split-band test. However, the effect on the RCS scaling value can be neglected. From Figure 13(b), it can be observed that the RCS reduction values are higher than 10 dB in

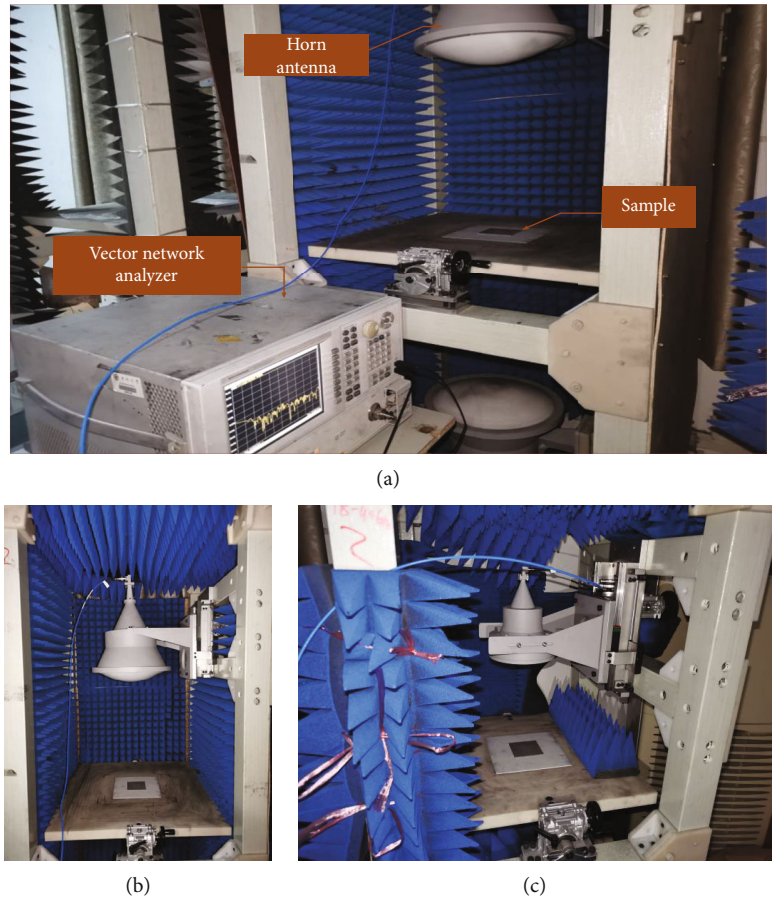

FIGURE 12: (a) Experimental test environment and equipment. (b) 8-18 GHz low-frequency test. (c) 18-40 GHz high-frequency test.

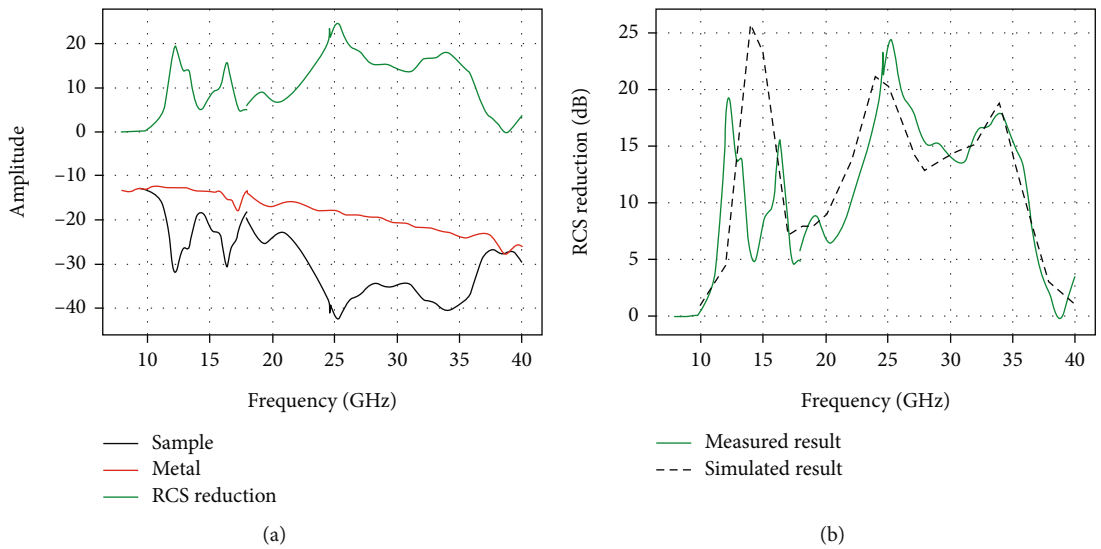

FIGURE 13: (a) Experimental test data of RCS reduced surface sample and metal plate experimental test. (b) Comparison of experimental and simulation data.

the three frequency bands of 12-14 GHz, 15.8-16.5 GHz, and 22.5-36.3 GHz. We have compared our supersurface properties with the literature cited in the manuscript as shown in Table 1. This test environment is referenced from the literature [36, 37]. The scaling trends of experimental results and simulation results in the high-

Table 1: Performance comparison of proposed metasurface in the literature for RCS reduction.

Ref.	RCS reduction (dB)	Frequency band (GHz)	Unit size (mm)	Angular (deg)
[24]	10	8-24	3×3	45
[25]	7.5	7-18	12×12	60
[26]	5	8-14	8.3×8.3	60
[31]	10	3.5-16.6	12×12	No mention
[32]	10	18-34	4.9×4.9	45
[38]	10	4.3-16.5	14×14	30
Our work	10	12.5-17.4 & 20.5-36.2	5×5	70

frequency band are consistent, and there are large differences in the low-frequency band, which are analyzed for the following reasons: (1) The sample plate size is small, and the wavelength in the low-frequency band is relatively long. Therefore, the experimental error will become larger during the test. (2) The precision of the sample plate processing may not be enough.

4. Conclusion

Based on electromagnetic metamaterials, we explored and designed a new type of RCS reduction metasurface that achieves RCS reduction in a wide frequency range. The polarization conversion unit is used as a 1-bit coding unit, with two polarization conversion units representing units "1" and "0." The genetic algorithm is used to optimize the design of the coding sequence of the RCS reduction metasurface. CST simulation was used to verify that the optimized RCS reduction surface can reduce RCS in a wide frequency range from 10 to 40 GHz. A metasurface model with the same size as the simulation model was fabricated, and the RCS reduction function of the model was tested in a microwave darkroom. Both simulation and experimental results demonstrate that the designed RCS reduction metasurface has a good RCS reduction effect and a wider frequency band and exhibits a better reduction effect under wide-angle oblique incidence. Compared with a metal plate of the same size, the RCS reduction metasurface can achieve an RCS reduction of more than 10 dB in two frequency bands, namely, 12.5-17.4 GHz and 20.5-36 GHz, with relative bandwidths of 32.78% and 56.30%, respectively. The maximum reduction reaches 26 dB, which proves that the RCS reduction metasurface can effectively reduce the RCS.

Data Availability

The data used to support the findings of this study are included in the article. If the reader needs more detail, they can contact the first author only by email (510036270@qq.com).

Conflicts of Interest

The authors declare that they have no conflicts of interest.

Acknowledgments

This study is supported by the National Cultivation Project of China West Normal University (grant number: 19B025) and by the Sichuan College Students' Innovation and Entrepreneurship Training program (grant numbers: S202110638103X and S202210638038X). Nanchong key laboratory foundation "Electromagnetic Engineering and Technology" also supports this work.

References

[1] J. I. Weixiang, T. I. Hanwei, S. O. Chao, and Z. H. Xin'ge, "Digital coding metasurfaces: toward programmable and smart manipulations of electromagnetic functions," *Journal of Radars*, vol. 11, no. 6, pp. 1003–1019, 2022.

[2] R. A. Shelby, D. R. Smith, and S. S. And, "Experimental verification of a negative index of refraction," *Science*, vol. 292, no. 5514, pp. 77–79, 2001.

[3] D. Schurig, J. J. Mock, B. J. Justice et al., "Metamaterial electromagnetic cloak at microwave frequencies," *Science*, vol. 314, no. 5801, pp. 977–980, 2006.

[4] M. Silveirinha and N. Engheta, "Tunneling of electromagnetic energy through subwavelength channels and bends using ε-near-zero materials," *Physical Review Letters*, vol. 97, no. 15, article 157403, 2006.

[5] R. Liu, Q. Cheng, T. Hand et al., "Experimental demonstration of electromagnetic tunneling through an epsilon-near-zero metamaterial at microwave frequencies," *Physical Review Letters*, vol. 100, no. 2, article 023903, 2008.

[6] H. L. Zhu, S. W. Cheung, K. L. Chung, and T. I. Yuk, "Linear-to-circular polarization conversion using metasurface," *IEEE Transactions on Antennas and Propagation*, vol. 61, no. 9, pp. 4615–4623, 2013.

[7] P. Xu, G. C. Wang, X. Cai, H. Y. Shen, and W. X. Jiang, "Design and optimization of high-efficiency meta-devices based on the equivalent circuit model and theory of electromagnetic power energy storage," *Journal of Physics D: Applied Physics*, vol. 55, no. 19, article 195303, 2022.

[8] Z. Wang, X. Ding, K. Zhang et al., "Huygens metasurface holograms with the modulation of focal energy distribution," *Advanced Optical Materials*, vol. 6, no. 12, article 1800121, 2018.

[9] G. Zheng, H. Mühlenbernd, M. Kenney, G. Li, T. Zentgraf, and S. Zhang, "Metasurface holograms reaching 80% efficiency," *Nature Nanotechnology*, vol. 10, no. 4, pp. 308–312, 2015.

[10] N. M. Estakhri and A. Alù, "Wave-front transformation with gradient metasurfaces," *Physical Review X*, vol. 6, no. 4, article 041008, 2016.

[11] V. S. Asadchy, M. Albooyeh, S. N. Tcvetkova, A. Díaz-Rubio, Y. Ra'di, and S. A. Tretyakov, "Perfect control of reflection and refraction using spatially dispersive metasurfaces," *Physical Review B*, vol. 94, no. 7, article 075142, 2016.

[12] S. Yan, M. Haoxuan, and H. Wang, "Polarization conversion metasurface design based on characteristic mode rotation and its application into wideband and miniature antennas with a low radar cross section," *Optics Express*, vol. 29, no. 5, pp. 6794–6809, 2021.

[13] Y. M. Liu and X. Zhang, "Metamaterials: a new frontier of science and technology," *Chemical Society Reviews*, vol. 40, no. 5, pp. 2494–2507, 2011.

[14] W. Long, W. Liuying, L. Gu et al., "Study on the optical stealth characteristics of micro/nano structure of Morpho Menelaus wing scales," *Rare Metal Materials and Engineering*, vol. 51, no. 5, pp. 1926–1CP3, 2022.

[15] L. Yan, X. Wang, S. Zhao et al., "Highly efficient microwave absorption of magnetic nanospindle–conductive polymer hybrids by molecular layer deposition," *ACS Applied Materials & Interfaces*, vol. 9, no. 12, pp. 11116–11125, 2017.

[16] J. Li and J. Pendry, "Hiding under the carpet: a new strategy for cloaking," *Physical Review Letters*, vol. 101, no. 20, article 203901, 2008.

[17] J. B. Pendry, D. Schurig, and D. R. Smith, "Controlling electromagnetic fields," *Science*, vol. 312, no. 5781, pp. 1780–1782, 2006.

[18] R. B. Greegor, C. G. Parazzoli, J. A. Nielsen, M. A. Thompson, M. H. Tanielian, and D. R. Smith, "Simulation and testing of a graded negative index of refraction lens," *Applied Physics Letters*, vol. 87, no. 9, article 091114, 2005.

[19] A. Alu, M. G. Silveirinha, A. Salandrino, and N. Engheta, "Epsilon-near-zero metamaterials and electromagnetic sources: tailoring the radiation phase pattern," *Physical Review B*, vol. 75, no. 15, article 155410, 2007.

[20] R. Liu, C. Ji, J. J. Mock, J. Y. Chin, T. J. Cui, and D. R. Smith, "Broadband ground-plane cloak," *Science*, vol. 323, no. 5912, pp. 366–369, 2009.

[21] D. Priyanka and M. Kaushik, "RCS reduction of microstrip antenna using split square loop thin absorber," *IET Microwaves, Antennas & Propagation*, vol. 14, no. 14, pp. 1771–1778, 2020.

[22] S. Li, Z. Li, X. Liu et al., "Transmissive digital coding metasurfaces for polarization-dependent dual-mode quad orbital angular momentum beams," *ACS Applied Materials & Interfaces*, vol. 15, no. 19, pp. 23690–23700, 2023.

[23] J. Su, H. He, Z. Li, Y. Yang, H. Yin, and J. Wang, "Uneven-layered coding metamaterial tile for ultra-wideband RCS reduction and diffuse scattering," *Scientific Reports*, vol. 8, no. 1, p. 8182, 2018.

[24] J. Yang, Y. Pang, J. Wang et al., "Achieving broadband RCS reduction using carbon fiber connected composite via scattering mechanism," *Composites Science and Technology*, vol. 200, article 108410, 2020.

[25] H.-X. Xu, S. Ma, X. Ling et al., "Deterministic approach to achieve broadband polarization-independent diffusive scatterings based on metasurfaces," *ACS Photonics*, vol. 5, no. 5, pp. 1691–1702, 2018.

[26] H. X. Xu, L. Zhang, Y. Kim et al., "Wavenumber-splitting metasurfaces achieve multichannel diffusive invisibility," *Advanced Optical Materials*, vol. 6, no. 10, pp. 1800010.1–1800010.9, 2018.

[27] H. X. Xu, M. Wang, G. Hu et al., "Adaptable invisibility management using kirigami-inspired transformable metamaterials," *Research*, vol. 2021, no. 1, Article ID 9806789, 11 pages, 2021.

[28] Y. Guo, L. Yan, W. Pan, and L. Shao, "Scattering engineering in continuously shaped metasurface: an approach for electromagnetic illusion," *Scientific Reports*, vol. 6, no. 1, article 30154, 2016.

[29] H. Dai, Y. Zhao, H. Li, J. Chen, Z. He, and W. Qi, "An ultra-wide band polarization-independent random coding metasurface for RCS reduction," *Electronics*, vol. 8, no. 10, p. 1104, 2019.

[30] S. J. Li, B. W. Han, Z. Y. Li et al., "Transmissive coding metasurface with dual-circularly polarized multi-beam," *Optics Express*, vol. 30, no. 15, pp. 26362–26376, 2022.

[31] K. Chen, W. Guo, G. Ding, J. Zhao, T. Jiang, and Y. Feng, "Binary geometric phase metasurface for ultra-wideband microwave diffuse scatterings with optical transparency," *Optics Express*, vol. 28, no. 9, pp. 12638–12649, 2020.

[32] W. Ying-Jie, C. Ke, Z. Fang-Kun, T. Jiang-Xiao, F. Yu-Feng, and C. Ping, "Resonance phase and geometric phase integrated diffusion metasurface for broadband scattering control," *Journal of Physics D: Applied Physics*, vol. 54, no. 16, article 165101, 2021.

[33] T. J. Cui, M. Q. Qi, X. Wan, J. Zhao, and Q. Cheng, "Coding metamaterials, digital metamaterials and programmable metamaterials," *Light: Science & Applications*, vol. 3, no. 10, pp. e218–e218, 2014.

[34] L. Zakaria and C. Salim, "Comparison of genetic algorithm and quantum genetic algorithm," *The International Arab Journal of Information Technology*, vol. 9, no. 3, pp. 243–249, 2020.

[35] A. Baykasoglu and C. Baykasoglu, "Multiple objective crashworthiness optimization of circular tubes with functionally graded thickness via artificial neural networks and genetic algorithms," *Proceedings of the Institution of Mechanical Engineers, Part C: Journal of Mechanical Engineering Science*, vol. 23, no. 1, pp. 2005–2016, 2020.

[36] H. L. Wang, H. F. Ma, M. Chen, S. Sun, and T. J. Cui, "A reconfigurable multifunctional metasurface for full-space control of electromagnetic waves," *Advanced Functional Materials*, vol. 31, no. 25, article 2100275, 2021.

[37] Z. Luo, M. Z. Chen, Z. X. Wang et al., "Digital nonlinear metasurface with customizable nonreciprocity," *Advanced Functional Materials*, vol. 29, no. 49, article 1906635, 2019.

[38] X. He, C. Qi, and A. M. H. Wong, "A compact transparent polarization-insensitive metasurface with broadband monostatic and bistatic radar cross-section reduction of millimeter-waves," *Journal of Physics D: Applied Physics*, vol. 55, no. 35, article 355104, 2022.